DOI: 10.1002/ejic.200900371

Peptization–Hydrothermal Method as a Surfactant-Free Process toward Nanorod-Like Anatase TiO_2 Nanocrystals

Shuang Li,[a] Yaogang Li,[b] Hongzhi Wang,*[a] Wugang Fan,[c] and Qinghong Zhang*[b]

Keywords: Nanostructures / Hydrothermal synthesis / Sol-gel processes / Crystal growth / Titanium

The transparent TiO_2 sol contained of anatase crystallites was prepared by peptization of anatase TiO_2 precipitates. With the hydrothermal treatment of TiO_2 sol at 150 °C, the dispersible and nanorod-like TiO_2 nanocrystals were formed by an oriented attachment mechanism. After further hydrothermal treatment of the mixture of nanorod-like TiO_2 nanocrystals and the original sol, branched and nanoring-like nanostructures in the anatase phase were obtained. The as-prepared TiO_2 nanocrystals were characterized by X-ray diffraction, FT-Raman spectrometry, UV/Vis absorption spectrometry, and transmission electron microscopy (TEM). TEM results indicated that TiO_2 nanocrystals were nanorod-like, and more complex microstructures such as the ring-like and branched TiO_2 nanostructures with diameters less than 10 nm were formed especially in the two-step hydrothermal treatment. The adsorption of ruthenium dye (N719) over the nanocrystals with different microstructures was investigated. The adsorption results showed the nanorod-like anatase TiO_2 nanocrystals had a high capacity for the ruthenium dye adsorption. The powders were used as electrodes of dye-sensitized solar cells and showed a conversion efficiency of 5.75 % under 1 sun illumination unit of simulated sunlight.

Introduction

Titanium dioxide is widely used as a whitening pigment, in electroceramic materials and catalyst supports, and as a photocatalyst.[1] In recent years, nanocrystalline TiO_2 materials have attracted attention in various fields of science and technology because of their unique property that the crystallite size has a significant quantum confinement effect with a typical dimension less than 10 nm.[2–4] For applications in dye-sensitized solar cells (DSSCs) and in photocatalysis, the size- and shape-dependent properties of nanostructured TiO_2 are demonstrated.[4–8] Therefore, to optimize the performance of TiO_2, it is essential to be able to control the crystallite size, the phase, and the morphology of nanostructured TiO_2. Recently, a network-like TiO_2 film was used as a photoelectrode for DSSCs, and it was prepared by the thermal hydrolysis of titanium alkoxide at 80 °C; it showed an enhanced photoelectrical conversion efficiency as high as 9.3% under 1 sun illuminating unit.[3,9]

There are various routes to prepare TiO_2 nanocrystals, including sol–gel processes, micelle and microemulsion syntheses, nonhydrolytic syntheses, heat-injection syntheses, hydrothermal processes, and so on.[4,10] In these processes, the hydrothermal process is the most versatile method; titanium salts usually hydrolyze in solution and then crystallize into the anatase or rutile phase. Also, amorphous TiO_2 precipitates transform into anatase or rutile TiO_2 nanocrystals depending on the acidity of the dispersion during the hydrothermal treatment.[11] Brinker et al. reported the relationship between the TiO_2 electrode microstructure and properties for dye-sensitized solar cells; the nanocrystalline TiO_2 was obtained by modifying titanium isopropoxide with acid as titanium precursors following the hydrothermal treatment.[12] Yuwono et al. improved the TiO_2 crystallinity in the nanohybrid thin films through the hydrothermal treatment in high-pressure water vapor at 150 °C.[13] Andersson et al. synthesized TiO_2 nanoparticles of both anatase and rutile phases by hydrothermal treatment of microemulsions.[14] Kolen'ko et al. investigated a formation process of TiO_2 nanorods starting from the titanate fibers during hydrothermal synthesis.[15] Sugimoto et al. developed a gel–sol process to prepare TiO_2 or Fe_2O_3 nanocrystals with a controllable size or shape.[16–18] A new mechanism involving oriented attachment in relation to the formation of semiconductor nanorods has been presented by Penn and Banfield for the first time.[19–21] Despite the recent efforts devoted to the synthesis TiO_2 nanocrystals using hydrothermal processes, the crystallite size is not extremely small (less

[a] State Key Laboratory for Modification of Chemical Fibers and Polymer Materials, Donghua University,
Shanghai 201620, P. R. China
E-mail: wanghz@dhu.edu.cn
[b] Engineering Research Center of Advanced Glasses Manufacturing Technology, MOE, Donghua University,
Shanghai 201620, P. R. China
Fax: +86-21-67792855
E-mail: zhangqh@dhu.edu.cn
[c] Shanghai Institute of Ceramics, Chinese Academy of Sciences,
Shanghai 200050, P. R. China

than 10 nm). In the other routes to prepare TiO_2, uniform TiO_2 nanorods were successfully obtained.[22–26] For example, Chemseddine and Thomas prepared anatase TiO_2 in the presence of tetramethylammonium hydroxide,[24] whereas Wu et al. prepared the self-aggregated rutile TiO_2 through a sol–hydro(solvo)thermal route.[25] However, the commonly used surfactants to control the crystal growth shape and size may be detrimental to the photocatalytic and adsorptive properties.[26] Therefore, it is still a challenge to obtain desired sizes and microstructures of TiO_2 nanocrystals through the hydrothermal method by a surfactant-free process.

In the present work, we describe a peptization and two-step hydrothermal process for the synthesis of nanorod-like anatase TiO_2 nanocrystals with a high aspect ratio without any organic surfactants. First, the transparent anatase TiO_2 sol was prepared by peptization, and subsequently the sol was subjected to hydrothermal treatment. On the basis of the oriented attachment mechanism, nanorod-like anatase TiO_2 nanocrystals were formed with diameters of about 6 nm and with an enhanced adsorptive capacity of the N719 dye. In contrast to the most-used amorphous TiO_2 sol derived from titanium alkoxide in an alcoholic solution, the crystallites were already in the anatase phase in the present work. The crystalline nature avoids exaggerated growth during the hydrothermal treatment,[11] and the surfactant-free surfaces of the TiO_2 nanocrystals are ideal for oriented attachment.

Results and Discussion

Absorption Spectra of Colloidal TiO2 Particles

The optical absorbance of TiO_2 sols diluted with deionized water is shown in Figure 1. Upon dilution of the sol with deionized water, the onset of adsorption appears at about λ = 370 nm. For the sol with a concentration less than 3.28 g L^{-1}, the optical absorption at $\lambda > 370$ nm is negligible (Figure 1d,e). There is a linear relationship between the absorbance and concentration of TiO_2: the absorbance gradually decreases as the diluted proportion increases, as illustrated in Figure 1B. As shown in the inset (Figure 1C), the sol was light-blue in color, which indicated the TiO_2 sol had a high transparency and was well dispersed in water. The UV/Vis absorption spectra of TiO_2 aqueous sol were similar to that of a TiO_2 sol reported by Liu and Claus,[2] both with a high transparency in the visible light region. Li et al. reported the UV/Vis spectra of well-dispersed anatase nanoparticles with a size of 7 nm at pH 3; some extinction in the visible light region was observed,[27] which is due to the scattering effect of the slightly aggregated nanoparticles. The sol was stable for several months at room temperature without any added organic stabilizers. There were no distinct differences between the UV/Vis absorption spectra of the sol and those after hydrothermal treatment as shown in Figure 1D, but the latter showed a stronger scattering effect in the visible light region. According to the work by Joo et al.,[26] one could estimate that the band gap of indirect semiconductor TiO_2 nanorods was 3.48 eV, and they showed a blueshift of 280 meV compared to bulk anatase TiO_2. A 130 meV blueshift was also observed for the anatase nanorods,[26] and we concluded that the blueshift of the band gap may mainly be dependent on the diameter of the nanorods rather than the length of the nanorods. So, the spherical anatase TiO_2 particles and the rod-like ones with a similar diameter showed identical spectra, and this result was consistent with the work on ligand-caped TiO_2 nanorods reported by Weller and co-workers.[22]

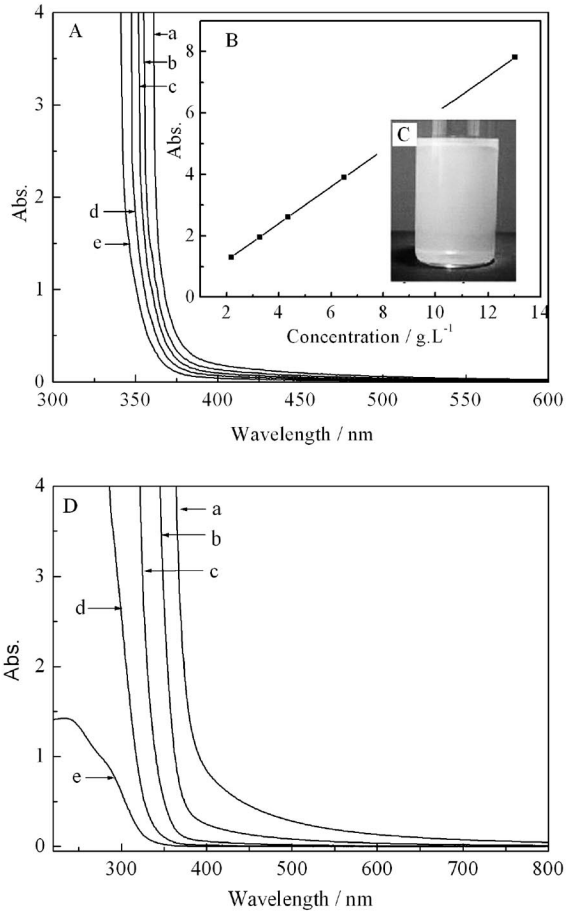

Figure 1. (A) UV/Vis absorption spectra of the TiO_2 sol with varying dilution. TiO_2 loading: (a) 13.04 g L^{-1}, (b) 6.52 g L^{-1}, (c) 4.24 g L^{-1}, (d) 3.28 g L^{-1}, and (e) 2.16 g L^{-1}. Insets: (B) the plot of the TiO_2 concentration and UV/Vis absorbance at λ = 365 nm and (C) the appearance of the primary sol without dilution. (D) UV/Vis absorption spectra of OSH TiO_2 with varying dilution. TiO_2 loading: (a) 13.75 g L^{-1}, (b) 2.75 g L^{-1}, (c) 0.5490 g L^{-1}, (d) 0.110 g L^{-1}, and (e) 0.0275 g L^{-1}.

XRD and Raman Analysis of the Crystallite Size in the Sols

The XRD patterns of the dried sol and one-step hydrothermal (OSH) and two-step hydrothermal (TSH) TiO_2 are shown in Figure 2, and all the diffraction peaks are assigned to the anatase phase of TiO_2, indicating perfect crys-

talline nature, in particular in the (101) plane. The XRD pattern shows broadened peaks compared to bulk anatase as a result of the significantly reduced crystallite size especially in Figure 2a. The average size of the TiO_2 nanoparticles in Figure 2a–c estimated from the Scherrer equation was about 4.7, 6.2, and 7.1 nm, respectively.

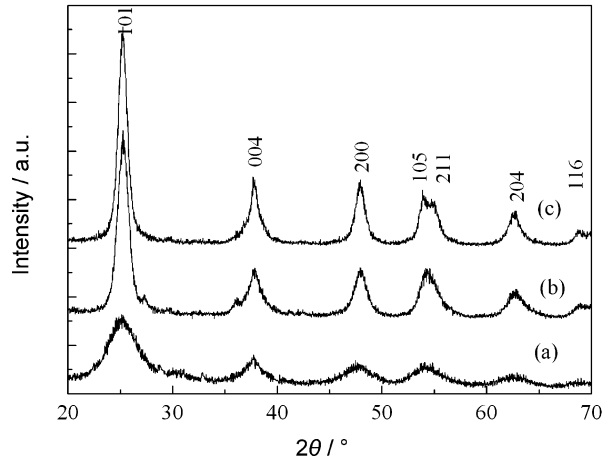

Figure 2. XRD pattern of samples: (a) the dried sol of TiO_2, (b) OSH TiO_2, and (c) TSH TiO_2.

Figure 3 shows the FT-Raman spectra of peptized sol and OSH and TSH TiO_2. The strongest Raman bands appeared at 159, 148, and 148 cm^{-1} for the dried sol, OSH TiO_2, and TSH TiO_2, respectively. Compared to the E_g mode of bulk anatase TiO_2 at 144 cm^{-1}, the frequency shifts observed are about 15, 4, and 4 cm^{-1}, respectively. The shift of E_g to higher frequency is characteristic of anatase TiO_2 nanocrystals in the ultrafine size.[28] It shifted towards the red region, which corresponds to the distinct broadening of the half width at half maximum (HWHM) signal with decreasing size of the of the crystallite. According to the result reported by Kelly et al.,[28] one can calculate the particle size of TiO_2 in the sol and OSH and TSH TiO_2 to be 4.2, 6.5, and 6.5 nm, respectively. Their crystallite sizes calculated on the basis of the shift of the strongest E_g mode

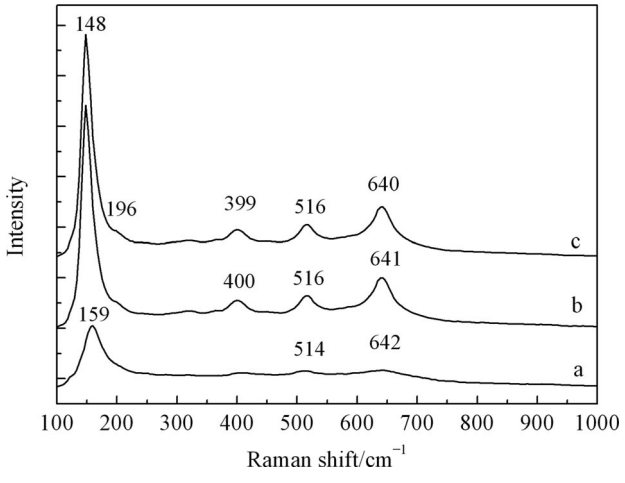

Figure 3. FT-Raman spectra of (a) TiO_2 sol, (b) OSH TiO_2, and (c) TSH TiO_2.

in the Raman spectra are close to the sizes calculated with the Scherrer equation. The result of the Raman spectra indicated the coarsening of the TiO_2 crystallites during the hydrothermal treatment, although after hydrothermal treatment the TiO_2 crystallites were much finer than by hydrothermal treatment of amorphous precipitates, titanium salts, or titanium alkoxides.[11,15,29] It may be explained by the fact that the crystalline nature of anatase TiO_2 in the sol prevented exaggerated growth, which is generally observed in the transformation of the amorphous solid into the anatase phase during the hydrothermal process.[11]

TEM Characterization of the Crystallite Size in the Sols

TEM micrographs of the samples are given in Figure 4. Most of the nanoparticles have elongated rod-like morphologies, and they are connected to each other to form a rod-like shape. Almost no isolated particles were observed; rod-like nanocrystals with a diameter of about 6 nm were formed, and they had a crystalline nature of anatase phase with good dispersible ability (Figure 4a). It is noted that these rod-like nanocrystals were not of uniform diameter, but instead they possessed a zigzag diameter, as shown in the HRTEM images (Figure 4b,c), which is typical for nanorods formed by the mechanism of oriented attachment (OA).[20] The rod-like nanocrystals were of perfect single-crystal nature, which grew along the *c* axis (Figure 4b) or exposed with (101) plane (Figure 4c).

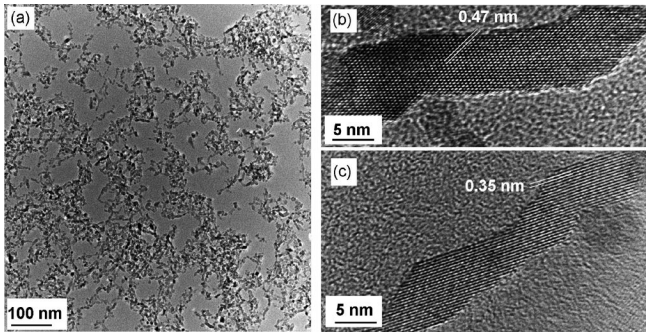

Figure 4. TEM and HRTEM images of OSH TiO_2. (a) Low-magnification TEM, (b) high-resolution TEM image of TiO_2 rod-like nanocrystals along the *c* axis with the exposed (002) plane, and (c) high-resolution TEM image of TiO_2 rod-like nanocrystals with the exposed (101) plane.

From the TEM image of TSH TiO_2 (Figure 5a) it is noted that TiO_2 had a complex nanoring-like consisting of rod-like nanocrystals with diameters of about 6 nm. The HRTEM image of typical TiO_2 nanostructure in TSH TiO_2 is shown in Figure 5b–d, and it reveals that nanoparticles aligned along crystal growth with a high aspect ratio by the oriented attachment mechanism, and formed the nanoring-like (Figure 5b), rod-like (Figure 5c), and T-type (Figure 5d) structures. As we expected, after hydrothermal treatment of the mixture of anatase TiO_2 rod-like nanocrystals with the original sol, the spherical nanoparticles may collide with the already formed rod-like nanocrystals (Brownian motion) and cohere with each other. When they

were with the oriented crystallographic plane, more complex structures such as nanoring-like and T-type TiO_2 nanostructures were formed. By counting the number of the primary crystallites formed in the nanoring-like structures, one can estimate that about 20% nanocrystals were orientationally attached to the closed and near-closed nanorings, as showed in Figure 5a. In the single-crystal rod-like nanocrystals, angles of 45 or 135° between the primary particles predominantly occurred, corresponding to the angle between the (101) plane with the *a* axis of anatase TiO_2.

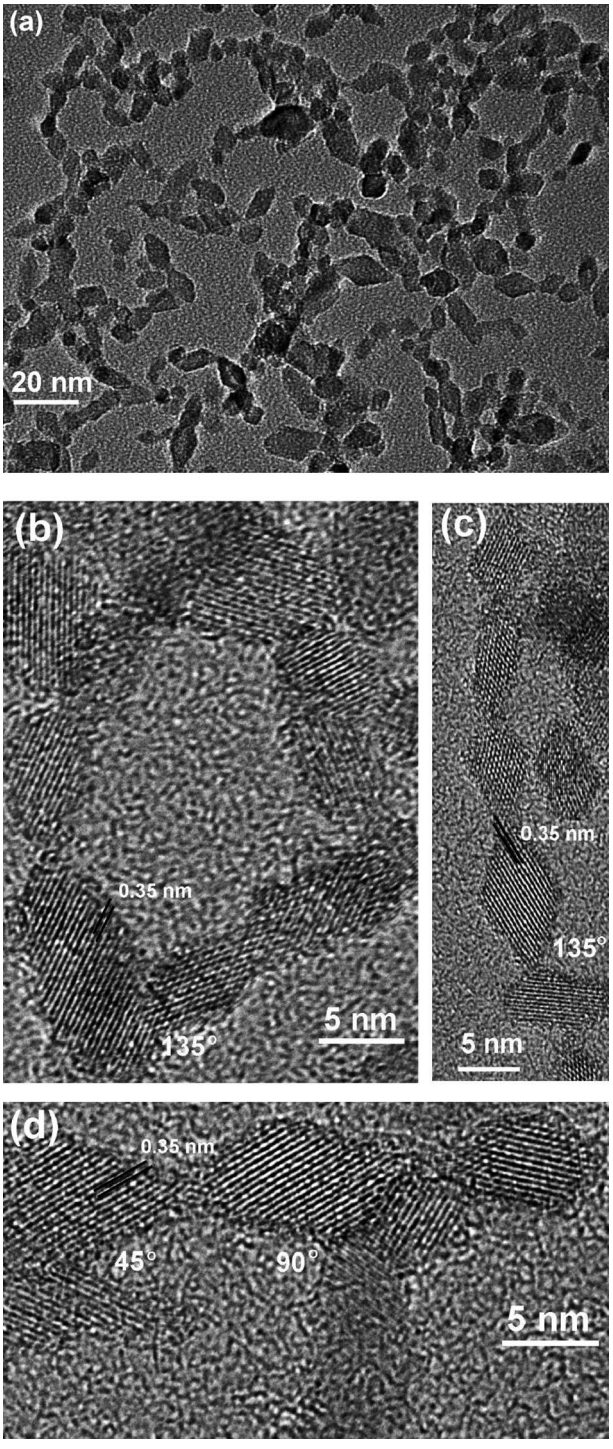

Figure 5. TEM and HRTEM images of TSH TiO_2. (a) Low-magnification TEM, (b) HRTEM image of nanoring-like TiO_2, (c) HRTEM image of TiO_2 nanorod by the oriented attachment of six primary nanocrystals, and (d) HRTEM image of T-type TiO_2 nanocrystals; it also contains the attachment with an angle of 45°.

Formation Mechanism of the Anatase TiO2 Rod-Like Nanocrystals

The OA mechanism was recently found to be significant in the growth of nanomaterials as an approach for the preparation of complex nanostructures.[19–21,30–32] In this synthesis, there are the anatase crystallites in the precipitate obtained at 70 °C prior to peptization.[33] The peptization process destroys agglomerates during precipitation. The needed energy for deagglomeration was supplied by heating, and the precipitate in the presence of HNO_3 transformed into the well-dispersed sol. During autoclaving, the primary particles can somewhat grow through the dissolution–reprecipitation process under hydrothermal conditions, leading to some coarsening of the crystallite size. In this work, the sol was diluted with deionized water before autoclaving, and the concentration of H^+ is of about 0.1 M. A pH value of 1.0 in the diluted sol was achieved; however, it is still far from the isoelectric point of TiO_2 (pH 6) at room temperature and also more acidic than the optimized acidic conditions for the OA growth of TiO_2 (0.001 M HCl) suggested by Penn and Banfield.[20] However, there is a much lower isoelectric point of TiO_2 under hydrothermal conditions as suggested by Penn and Banfield[20] (i.e., pH 3 for anatase {112} surfaces). Also, the gel-like precipitates rather than the well-dispersed colloids indicated the aggregating of TiO_2 nanocrystals under hydrothermal conditions. Compared to the hydrothermal conditions, we assume that the highly concentrated TiO_2 sol was used in the present work (in the Penn and Banfield work, the TiO_2 concentration was 3 mg g^{-1} or 0.0375 M), and the ratio of TiO_2 to H^+ also plays an important role in the oriented attachment besides the pH value. The higher the TiO_2 concentration in the sol the higher the chances that TiO_2 nanocrystals collide with the aligned crystallographic surfaces.[31,32] Under more acidic conditions, some anatase TiO_2 nanocrystals in a finer size may dissolve under the Ostwald ripening mechanism, which produces the dissolved Ti species for both the growing of anatase nanocrystals and the perfect junctions of TiO_2 with the aligned crystallographic surfaces. The growth of the nanoparticles with rod-like morphologies is clearly observed in Figure 4b,c, and the diameter was of 6–7 nm, which is larger than the 5 nm observed in the original sol. During the two-step hydrothermal autoclaving of the mixture of OSH-derived, rod-like nanocrystals with the original sol, some anatase TiO_2 may attach and grow around those already formed rod-like nanocrystals, so higher aspect ratio rod-like nanocrystals and more complex structure for the OA growth were expected in the two-step hydrothermal treatment. Indeed, the longer rod-like nanocrystals, branched rod-like nanocrystals, and nanoring-like struc-

tures were formed, and the HRTEM image shows a nanoring-like structure from the two-step hydrothermal treatment (Figure 5b–d).

Adsorptive Property of N719 Dye

Anatase TiO_2 nanocrystals have a promising application in the dye-sensitized solar cells as a photoelectrode. Generally, a paste of nanocrystalline TiO_2 is coated onto a transparent conductive oxide such as indium tin oxide (ITO) or fluoride-doped tin oxide (FTO) and then subsequently subjected to sintering at about 450 °C for 0.5 h. Figure 6 shows the adsorption isotherms of N719. The adsorption experiment of calcined TiO_2 powders were carried out at room temperature by using a typical ruthenium dye to reveal the surface adsorption properties. The dye uptake amounts on per BET surface area of anatase nanocrystals are given in Figure 6. A relative high adsorptive capacity of anatase TiO_2 for the adsorption of N719 was observed,[34] and the experimental data fit Langmuir isotherm.[9] It can be found that the uptake of N719 dye over OSH TiO_2 is slightly larger than TSH TiO_2, suggesting that the adsorption capacity of N719 on OSH TiO_2 surface is slightly stronger than those of TSH TiO_2. After calcinations at 450 °C for 30 min, the specific surface area of one-step hydrothermal and two-step hydrothermal TiO_2 are 115 and 108 $m^2 g^{-1}$, respectively. On the basis of the weight of both samples, the one-step hydrothermal TiO_2 has a higher capacity for the N719 dye. The TSH TiO_2 has an adsorption capacity of 0.50 molecule nm^{-2}, which is two times higher than 0.24 molecule nm^{-2} for the commercial TiO_2 nanocrystals ST-01.[34]

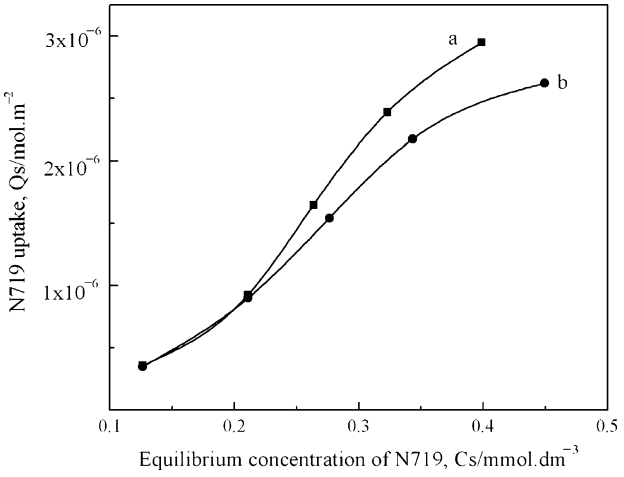

Figure 6. Isotherms for N719 dye adsorption on (a) OSH TiO_2 and (b) TSH TiO_2.

The N719-sensitized TiO_2 solar cells were characterized by measuring their current–voltage behavior by using a black metal mask with an aperture area of 0.16 cm^2 under standard AM 1.5 simulated sunlight (power density of 1000 W m^{-2}). The typical current density versus voltage curves of the TSH TiO_2, Ti15012h, and Ti20012h samples with thicknesses of 10 μm are shown Figure 7. Although the BET specific surface area of TSH TiO_2 is lower than that of Ti20012h and only half of Ti15012h, its electrode showed a short-circuit density of 12.2 mA cm^{-2} and a conversion efficiency (η) of 5.75 ± 0.06%. The η of Ti15012h and Ti20012h is of 5.71 ± 0.06 and 6.12 ± 0.08%, respectively. The current density is comparable to that mesoporous TiO_2 beads reported by Caruso et al. very recently.[35] The charge recombination sites have been suggested to lead to a decrease in open-circuit voltage (V_{oc}), which should occur mainly at nanocrystalline TiO_2/redox electrolyte interfaces;[36] thus, the cites in TSH TiO_2 were less than the other ones. Among them, TSH TiO_2 showed the highest V_{oc} of 681 mV but was still lower that of mesoporous TiO_2 beads of 800 mV,[35] and the work to raise the V_{oc} is under investigation in our lab.

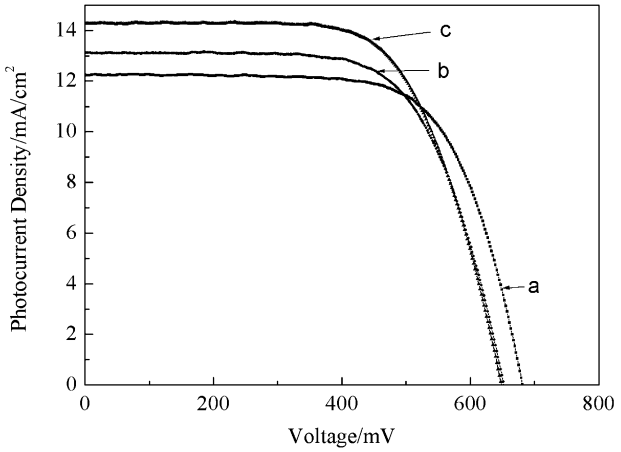

Figure 7. Current–voltage curves of the TiO_2 electrodes from (a) TSH TiO_2, (b) Ti15012h and (c) Ti20012h. Ti15012h and Ti20012h were hydrothermally treated with nondiluted sols at 150 and 200 °C for 12 h, and they had a BET specific surface area of 226 and 126 $m^2 g^{-1}$, respectively.

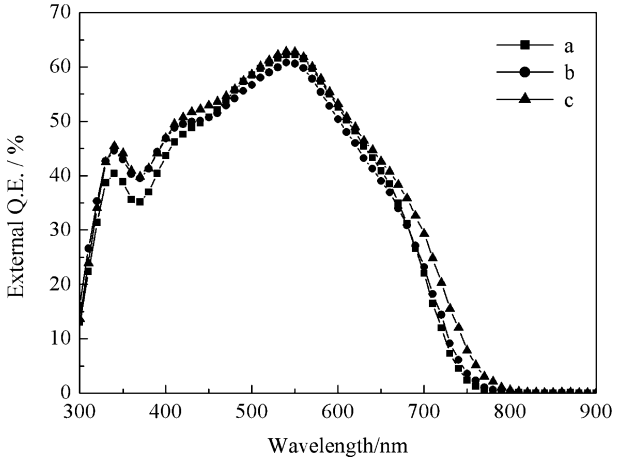

Figure 8. Incident photon to current conversion efficiency (IPCE) curves of the TiO_2 electrodes from (a) TSH TiO_2, (b) Ti15012h, and (c) Ti20012h.

Figure 8 displays the incident photon to current efficiency (IPCE) spectra for the several DSSCs. The quantum efficiency of all cells with N719 dye were maximized at around 550 nm, and external quantum efficiency approach the recently reported IPCE values.[35] For TSH TiO_2, the peak efficiency was slightly lower than that of Ti20012h but similar to that of Ti15012h. As a result, similar η values were obtained for DSSCs from TSH TiO_2 and Ti15012h. The trend of IPCE results according to TiO_2 structures are quite consistent with η values determined by I/V curves.

Conclusions

In summary, the organic-free and anatase TiO_2 sol with a higher concentration, improved stability, and high transparency was prepared by peptization of the precipitates containing anatase TiO_2. The anatase rod-like nanocrystals and more complex microstructures such as the nanorings were formed during subsequent hydrothermal treatment through an oriented-attachment mechanism. In the two-step hydrothermal treatment, a much higher concentration of TiO_2 sol in a more acidic environment was used as the precursor for the anatase TiO_2 nanorod- and nanoring-like nanocrystals. This is crucial for the scale-up preparation and for the paste for the photoelectrode in DSSCs. Rod-like nanocrystals with diameters of about 6 nm were obtained, and they exhibited a high adsorptive capacity for the N719 dye.

Experimental Section

Colloid Synthesis: In a typical synthesis process, titanium sulfate (98%) was adjusted to 0.5 M as a stock solution with deionized water. Ammonia (2.0 M, 25–28 wt.-%, analytic grade, 250 mL) was slowly dropped into a violently stirring titanium sulfate solution, which was in advance heated to 70 °C, until the solution pH value was 7. As we previously reported, the precipitates at 70 °C from a titanium salt contained of mainly anatase TiO_2 in the presence of sulfate ions.[33] A white precipitate formed instantaneously, and a large amount of precipitate was obtained after ammonia solution was used up. The precipitate was collected by filtration and then washed with deionized water several times. One aliquot of the wet precipitate was peptized by adding HNO_3 (0.8 M, 65–68 wt.-%, analytic grade), and the mixture was heated at reflux at 70 °C to give a sol in slightly blue color. The titania content in the resulting sol was about 1.0 M, whereas the H^+ concentration was 0.5 M. Another aliquot was dried at room temperature the XRD and Raman analysis. For the hydrothermal treatment, the sol (10 mL) was diluted to 50 mL with deionized water (the concentration of TiO_2 is about 0.2 M), which was sealed in a Teflon-lined stainless steel autoclave (70 mL capacity) and maintained at 150 °C for 24 h. After cooling to room temperature, the gel-like precipitate was washed with deionized water until its pH value was about 7. Some of the TiO_2 gel was dried under vacuum and was ground into a fine powder for further characterization. This one-step hydrothermal (OSH) derived TiO_2 powder was referred to as OSH TiO_2 thereafter. For the two-step hydrothermal treatment, the well-washed gel was dispersed in water with a volume to 8 mL (during the washing process about 20% TiO_2 was lost, so the yield of TiO_2 in the washed gel was of 80%). This dispersion (5 mL) was mixed with the sol (5 mL), and the mixture was diluted to 50 mL with deionized water, followed by ultrasonication to a stable sol. The mixed sol was also at a concentration of 0.2 M on the basis of TiO_2. The sol was sealed in a Teflon-lined autoclave and maintained at 150 °C for 24 h once again. Finally, the mixture was cooled to room temperature, and the obtained gel-like precipitate was collected and rinsed with deionized water several times. This two-step hydrothermal (TSH) derived TiO_2 gel was dried under vacuum and was ground into a fine powder, and referred to as TSH TiO_2 thereafter.

Adsorption of N719 Dye on TiO_2 (Nanocrystals): When TiO_2 nanocrystals were used a photoelectrode for the DSSCs, it was sintered at the temperature about 450 °C and then the photoelectrode was sensitized a dye. So, in this work, both OSH and TSH TiO_2 were calcined at 450 °C for 0.5 h before the adsorption experiment. The calcined TiO_2 powders (20 mg) were added into an ethanol (10 mL) solution of *cis*-bis(thiocyanate)bis(2,2-bipyridyl-4,4-dicarboxylate) ruthenium(II) bistetrabutylammonium (N719, purchased from Solaronix Co.) dye at the concentration range from 2.0×10^{-4} to 1.0×10^{-3} M. Then the dye solution containing TiO_2 was statically placed at room temperature for 72 h for the saturated adsorption. After the adsorption, the powder was separated from the suspension by a centrifuge, and then the remaining N719 dye concentration in the supernatant was analyzed by using a Perkin–Elmer Lambda 35 (Perkin–Elmer, USA) spectrophotometer.

TiO_2 Electrode Preparation and Solar Cell Assembly: The solar cell was assembled by sandwiching the working and counter electrode with an electrolyte. To prepare the DSSSc working electrodes, the hydrothermal treated TiO_2 (1.0 g) was first dispersed into ethanol (9.0 mL) and sonicated for 30 min to form a paste. The TiO_2 paste was deposited by using a simple doctor-blade technique on sheet glass (Nippon Sheet Glass, Hyogo, Japan) that was coated with a fluorine-doped tin oxide (FTO) layer (sheet resistance of 15 Ω/□). The TiO_2 layer was dried in air at room temperature for 10 min, followed by treatment at 50 °C for 30 min. Then, the film was heated to 450 °C for 30 min before cooling to room temperature. The film of TiO_2 coating layer after calcination was 10 μm thick. Then, the electrode was immersed for 48 h in a solution of ruthenium dye N719 at a concentration of 3.0×10^{-4} M. The electrode was then rinsed with acetonitrile to remove excess amounts of dye and dried. A hotmelt polymer foil (Surlyn 1702, DuPont) was used a spacer frame between the electrode substrates. One drop of an iodine-based electrode solution was deposited onto the surface of the electrode and penetrated inside the TiO_2 film by capillary action. The electrolyte solution was composed of 600 M of 1,2-dimethyl-3-propylimidazolium iodide, 50 M iodine, 100 M of lithium iodide, and 500 M of *tert*-butylpyridine that was dissolved in acetonitrile (all the chemicals were purchased from Sigma–Aldrich Chemicals). The component of electrolyte was similar to the literature reported by Grätzel et al.[12] The counter electrode was platinized by applying a drop of 5 mM H_2PtCl_6 in 2-propanol onto a FTO glass substrate and annealing it in air at 400 °C for 10 min. The counter electrode was then clamped onto the top of the TiO_2 working electrode. Finally, a silver paste was added on clean areas of FTO glass to enhance conductivity and to ensure good contact during measurement. Three electrodes were made and tested for each case of TiO_2 sample to avoid misleading estimation of their performance. After the assembling, the solar cells were immediately measured the current–voltage (I/V) characteristic and incident photon to current conversion efficiency (IPCE); the reproducibility was good.

Characterization: The powder phase composition was identified by X-ray diffraction (XRD) equipment (Model D/max 2550 V, Rigaku

Co. Tokyo, Japan) by using Cu-K_α (λ = 1.5406 Å) radiation. The broadening of XRD peak at 2θ = 25.4° (d_{101}) for anatase TiO_2 was used to calculate the crystallite size according to the well-known Scherrer equation. Raman spectra were collected with a Fourier transform infrared-Raman spectrometer (NEXUS-5670, Nicolet, USA). The morphology and the size of the resultant titanium dioxide were observed by using transmission electron microscopy (JEM-2100F, JEOL Co., Japan). The UV/Vis absorption spectra were measured with a Lambda 35 spectrophotometer.

The photovoltaic properties of the solar cells were characterized by using a Zennium electrochemical workstation (Zahner-elecktrik GmbH & Co., Germany) under illumination of simulated sunlight provided by an Oriel solar simulator (Model 96160) with an AM 1.5 filter and a 300 W xenon lamp. The light intensity during the *I*/*V* characteristic was 1000 $W m^{-2}$, monitored with a Newport 1918-C power meter with 818P-030–18 PWR detector head. External quantum efficiency (EQE) also named as incident photon to current conversion efficiency (IPCE) plotted as a function of excitation wavelength from 300 to 900 nm were recorded on a specially designed IPCE system (CEP-1500, Bunkon-Keiki., Japan) for DSSCs. The working electrode was shielded by a black metal mask with an aperture of 0.16 cm^2.

Acknowledgments

This research is supported by the National Key Technology R & D Program (No. 2006BAA04B02-01), the National Natural Science Foundation of China (Nos. 50572116, 50772127, and 50772022), the Cultivation Fund of the Key Scientific and Technical Innovation Project (No. 708039), Shanghai Committee of Science and Technology (No. 05PJ14012), and Shanghai Leading Academic Discipline Project (B603).

[1] G. J. Wilson, G. D. Will, R. L. Frost, S. A. Montgomery, *J. Mater. Chem.* **2002**, *12*, 1787–1791.
[2] Y. J. Liu, R. O. Claus, *J. Am. Chem. Soc.* **1997**, *119*, 5273–5274.
[3] J. Jiu, S. Isoda, F. Wang, M. Adachi, *J. Phys. Chem. B* **2006**, *110*, 2087–2092.
[4] X. B. Chen, S. S. Mao, *Chem. Rev.* **2007**, *107*, 2891–2959.
[5] B. O'Regan, M. Grätzel, *Nature* **1991**, *353*, 734–740.
[6] L. Manna, E. C. Scher, A. P. Alivisatos, *J. Am. Chem. Soc.* **2000**, *122*, 12700–12706.
[7] S. A. Empedocles, R. Neuhauser, K. Shimizu, M. G. Bawendi, *Adv. Mater.* **1999**, *11*, 1243–1256.
[8] M. Nirmal, L. Brus, *Acc. Chem. Res.* **1999**, *32*, 407–414.
[9] M. Adachi, Y. Murata, J. Takao, J. Jiu, M. Sakamoto, F. Wang, *J. Am. Chem. Soc.* **2004**, *126*, 14943–14949.
[10] B. Koo, J. Park, Y. Kim, S.-H. Choi, Y.-E. Sung, T. Hyeon, *J. Phys. Chem. B* **2006**, *110*, 24318–24323.
[11] J. Ovenstone, K. Yanagisawa, *Chem. Mater.* **1999**, *11*, 2770–2774.
[12] C. J. Brinker, F. Arendse, P. Comte, M. Jirousek, F. Lenzmann, V. Shklover, M. Grätzel, *J. Am. Ceram. Soc.* **1997**, *80*, 3157–3171.
[13] A. H. Yuwono, Y. Zhang, J. Wang, X. H. Zhang, H. Fan, W. Ji, *Chem. Mater.* **2006**, *18*, 5876–5889.
[14] M. Andersson, L. Osterlund, S. Ljungstrom, A. Palmqvist, *J. Phys. Chem. B* **2002**, *106*, 10674–10679.
[15] Y. V. Kolen'ko, K. A. Kovnir, A. I. Gavrilov, A. V. Garshev, J. Frantti, O. I. Lebedev, B. R. Churagulov, G. Van Tendeloo, M. Yoshimura, *J. Phys. Chem. B* **2006**, *110*, 4030–4038.
[16] T. Sugimoto, X. P. Zhou, A. Muramatsu, *J. Colloid Interface Sci.* **2003**, *259*, 53–61.
[17] T. Sugimoto, X. P. Zhou, A. Muramatsu, *J. Colloid Interface Sci.* **2003**, *259*, 43–52.
[18] T. Sugimoto, X. P. Zhou, *J. Colloid Interface Sci.* **2002**, *252*, 347–353.
[19] R. L. Penn, J. F. Banfield, *Am. Mineral.* **1998**, *83*, 1077–1082.
[20] R. L. Penn, J. F. Banfield, *Geochim. Cosmochim. Acta* **1999**, *63*, 1549–1557.
[21] R. L. Penn, *J. Phys. Chem. B* **2004**, *108*, 12707–12712.
[22] P. D. Cozzoli, A. Kornowski, H. Weller, *J. Am. Chem. Soc.* **2003**, *125*, 14539–14548.
[23] Z. H. Zhang, X. H. Zhong, S. H. Liu, D. F. Li, M. Y. Han, *Angew. Chem. Int. Ed.* **2005**, *44*, 3466–3470.
[24] A. Chemseddine, M. Thomas, *Eur. J. Inorg. Chem.* **1999**, 235–245.
[25] X. F. Yang, H. Konishi, H. H. F. Xu, M. M. Wu, *Eur. J. Inorg. Chem.* **2006**, 2229–2235.
[26] J. Joo, S. G. Kwon, T. Yu, M. Cho, J. Lee, J. Yoon, T. Hyeon, *J. Phys. Chem. B* **2005**, *109*, 15297–15302.
[27] D. Bersani, P. P. Lottici, X.-Z. Ding, *Appl. Phys. Lett.* **1998**, *72*, 72–75.
[28] S. Kelly, F. H. Pollak, M. Tomkiewicz, *J. Phys. Chem. B* **1997**, *101*, 2730–2734.
[29] Q. H. Zhang, L. Gao, *Langmuir* **2003**, *19*, 967–971.
[30] J. X. Xu, L. P. Li, Y. J. Yan, H. Wang, X. X. Wang, X. Z. Fu, G. S. Li, *J. Colloid Interface Sci.* **2008**, *318*, 29–34.
[31] C. Ribeiro, E. J. H. Lee, T. R. Giraldi, E. Longo, J. A. Varela, E. R. Leite, *J. Phys. Chem. B* **2004**, *108*, 15612–15617.
[32] E. J. H. Lee, C. Ribeiro, E. Longo, E. R. Leite, *J. Phys. Chem. B* **2005**, *109*, 20842–20846.
[33] Q. H. Zhang, L. Gao, J. K. Guo, *J. Eur. Ceram. Soc.* **2000**, *20*, 2153–2158.
[34] P. Wen, H. Itoh, W. Tang, Q. Feng, *Langmuir* **2007**, *23*, 11782–11790.
[35] D. H. Chen, F. Z. Huang, Y. B. Cheng, R. A. Caruso, *Adv. Mater.* **2009**, DOI: 10.1002/adma.200802603.
[36] J. B. Xia, N. Masaki, K. J. Jiang, S. Yanagida, *Chem. Commun.* **2007**, 138–140.

Received: April 23, 2009
Published Online: August 4, 2009

